Available online at www.sciencedirect.com
ScienceDirect
Journal of Membrane Science 287 (2007) 138–145
journal of MEMBRANE SCIENCE
www.elsevier.com/locate/memsci

Influence of inorganic scalants and natural organic matter on nanofiltration membrane fouling

Chalor Jarusutthirak [a,*], Supatpong Mattaraj [b], Ratana Jiraratananon [c]

[a] *Department of Chemistry, Faculty of Science, King Mongkut's Institute of Technology Ladkrabang, Bangkok 10520, Thailand*
[b] *Department of Chemical Engineering, Faculty of Engineering, Ubon Ratchathani University, Ubon Ratchathani 34190, Thailand*
[c] *Department of Chemical Engineering, Faculty of Engineering, King Mongkut's University of Technology Thonburi, Bangkok 10140, Thailand*

Received 17 December 2005; received in revised form 6 September 2006; accepted 20 October 2006
Available online 25 October 2006

Abstract

The influence of inorganic scalants and NOM on nanofiltration (NF) membrane fouling was investigated by a crossflow bench-scale test cell. Mathematical fouling models were used to determine kinetics and fouling mechanisms of NF membrane. It was observed that, with natural organic matter (NOM) at a concentration of 10 mg L^{-1}, divalent cation, i.e. calcium (Ca^{2+}), exhibited greater flux decline than monovalent cation, i.e. sodium (Na^{+}), while solution flux curves dominated cake formation model, especially at high ionic strength. For inorganic scalants of polyanions, i.e. carbonate (CO_3^{2-}), sulphate (SO_4^{2-}), and phosphate (PO_4^{3-}), solution flux curves were relatively fitted well with pore blocking model, possibly due to precipitated species formed and blocked on membrane surface and/or pores. For different divalent cations (i.e. calcium and magnesium (Mg^{2+})), calcium showed greater flux decline than magnesium, possibly due to higher concentration of precipitated calcium species than that of precipitated magnesium species based on the pC (−log concentration) and pH diagram.

Keywords: Fouling; Fouling model; Inorganic scalants; Nanofiltration; Natural organic matter

1. Introduction

Nanofiltration (NF) membrane can be employed in several applications, including drinking water treatment, wastewater treatment and reclamation, as well as industrial water treatment, to produce high water quality. NF process in drinking water treatment is found to be very effective in removal of natural organic matters (NOM), as known as disinfection by-product (DBP) precursors during chlorination process. The NF membrane has also been applied to water softening due to rejection efficiency for monovalent and multivalent ions in hard water. A limitation in the use of NF process is potential of membrane fouling which significantly causes permeate flux decline, an increase of operation cost, and a decrease of membrane lifetime. The possible causes of NF membrane fouling depend on various factors, for example, membrane properties, feedwater characteristics, types of solutes, and operating conditions. Of these, NOM containing in feedwater is found as a major foulant for NF membrane [1,2]. Additionally, inorganic compounds can be responsible for flux decline. It was found that an increase of NaCl concentration or a presence of divalent cations increased membrane fouling [3]. Alkaline earth metal cations, for example, calcium (Ca^{2+}) and magnesium (Mg^{2+}) ions, led to more fouling problems on membrane when combined with polyanions, such as carbonate (CO_3^{2-}), sulphate (SO_4^{2-}), and phosphate (PO_4^{3-}) ions [4]. Membrane fouling characteristics were described by many researchers as pore blockage, pore constriction, and cake formation [5–8]. However, the fouling characteristics and influence of inorganic scalants with NOM on NF membrane fouling are required more exploration to be a basis of fouling prevention or membrane cleaning.

The objective of this study was to understand the influence of inorganic scalants and NOM on NF membrane fouling. Mathematical fouling models were used to determine kinetics of membrane fouling and to describe fouling behaviors during nanofiltraion, while the pC (−log concentration) and pH diagram was used to explain precipitated fouling on membrane surface.

* Corresponding author. Tel.: +66 2 326 4111x6245; fax: +66 2 326 4415.
E-mail address: kjchalor@kmitl.ac.th (C. Jarusutthirak).

0376-7388/$ – see front matter © 2006 Elsevier B.V. All rights reserved.
doi:10.1016/j.memsci.2006.10.034

2. Theory

2.1. Fouling models of dead-end operation

Hermia has developed mathematical fouling models to explain permeate flux reduction in the dead-end operation during filtration [5]. These fouling models have been used for further membrane research fields [6,7]. The mathematical fouling models based on dead-end operation can be illustrated as follows:

$$\frac{dJ_v}{dt} = -kJ_v(J_v)^{2-n} \quad (1)$$

where J_v is the solution (permeate) flux, k the rate constant or fouling coefficient, t the operating period and n is the dimensionless filtration constant: (1) cake formation model corresponds to $n=0$, (2) intermediate blocking model corresponds to $n=1$, (3) pore constriction or standard blocking model corresponds to $n=1.5$, and (4) complete pore blocking corresponds to $n=2.0$. For a dead-end operation, permeate flux caused by crossflow velocity is not included in the mathematical fouling models.

2.2. Fouling models of crossflow operation

The difference between dead-end and crossflow operation is caused by crossflow velocity on the membrane surface. For crossflow operation, the solution flux (J^*) associated with the back-transport mass transfer (i.e. crossflow velocity) is corporated in the fouling mechanism models. The mathematical models can be described in the following equations.

2.2.1. Pore blocking model (or complete pore blocking model)

The rate of change in the number of open pores is assumed to be proportional to the rate of particle convection to the membrane surface:

$$\frac{dJ_v}{dt} = -\frac{\alpha_{block} A_m C_{bulk} J_0}{n_0}(J_v - J^*) = -k_A(J_v - J^*) \quad (2)$$

where α_{block} is the pore blocking efficiency, C_{bulk} the concentration in the bulk solution, A_m the membrane area, J_0 the initial solution flux, J^* is solution flux associated with the back-transport mass transfer, n_0 the initial number of pores, and k_A is the kinetic rate for the pore blocking model (min^{-1}).

2.2.2. Pore constriction model (or standard blocking model)

The rate of change in the pore volume is assumed to relate to the rate of particle convection to the membrane surface:

$$\frac{dJ_v}{dt} = -\frac{(2\alpha_{pore} A_m C_{bulk} J_0)^{0.5}}{\pi r_0^2 \delta_m} J_v^{0.5}(J_v - J^*)$$
$$= -k_B J_v^{0.5}(J_v - J^*) \quad (3)$$

where α_{pore} is the standard pore block efficiency, r_0 the initial pore radius of membrane, and k_B is the kinetic rate for the pore constriction model ($LMH^{-0.5}\,min^{-1}$ or $m^{-0.5}\,min^{-0.5}$).

2.2.3. Intermediate blocking model

The rate of change in the cake thickness (limit on the membrane surface) is assumed to relate with the rate of particle convection to the membrane surface:

$$\frac{dJ_v}{dt} = -\frac{\alpha_{cake} R_c}{(R_m + R_c)\delta_c} A_m C_{bulk} J_v(J_v - J^*)$$
$$= -k_C J_v(J_v - J^*) \quad (4)$$

where α_{cake} is the specific resistance of cake layer ($m\,mg^{-1}$), δ_c the depth of the particle cake (m), R_m the resistance of the membrane (m^{-1}), R_c the resistance of the polarization and cake (m^{-1}), and k_C is the kinetic rate for the intermediate blocking model ($LMH^{-1}\,min^{-1}$ or m^{-1}).

2.2.4. Cake formation model

The hydraulic resistance caused by the particle cake is assumed to be proportional to the cake mass, m_{cake}:

$$\frac{dJ_v}{dt} = -\frac{\alpha_{cake} C_{bulk}}{R_m J_0} J_v^2(J_v - J^*) = -k_D J_v^2(J_v - J^*) \quad (5)$$

where α_{cake} is the specific resistance of cake layer ($m\,mg^{-1}$), and k_D is the kinetic rate for the cake formation model ($LMH^{-2}\,min^{-1}$ or $min\,m^{-2}$).

3. Experimental

3.1. Inorganic scalants

Inorganic scalants used in this study were NaCl, $CaCl_2$, $CaCO_3$, $Ca_3(PO_4)_2$, $CaSO_4{\cdot}2H_2O$, and $MgSO_4{\cdot}7H_2O$. Solutions having inorganic scalants were prepared for ionic strengths of 0.01 and 0.05 M. Conductivity meter was used to measure conductivity for feed solutions and samples during filtration.

3.2. Natural organic matter

Natural organic matter (NOM), obtained from surface water reservoir at Ubon Ratchathani's University, Thailand, was isolated by field reverse osmosis (RO) membrane. The isolation method was previously studied by Sun et al. [9] and Serkiz and Perdue [10]. The RO system was a polyamide thin-film composite (AG4040F) in a spiral wound crossflow configuration (GE Osmonics, USA.). The NOM rejection was about 99%. The DOC recovery was about 90.5% (not including DOC in permeate). For all filtration experiments, the concentrated NOM after RO isolation were diluted with DI water to prepare the NOM solution with a concentration of $10\,mg\,L^{-1}$ NOM, and pH of the solution was adjusted to 7.

3.3. Nanofiltration membrane

Thin-film polysulfone nanofiltration membrane, obtained from GE Osmonics, Inc., was used to determine system performance under crossflow operation system. This membrane has a model number of HL 2540F1072 (series 7933937). According

to the manufacturer's information, the membrane has a molecular weight cutoff (MWCO) of 150–300 Da, determined with uncharged organic molecules (i.e. glucose and sucrose compounds). The operating pH condition is in the range of 3.0–9.0 while the cleaning pH condition is in the range of 1.0–10.0. This membrane has relatively low for chlorine resistance about 0.1 ppm. The maximum operating temperature is about 50 °C. Nanofiltration membrane sheets were stored in 1% $Na_2S_2O_5$ and kept in 4 °C to minimize bacterial activities.

3.4. Crossflow bench-scale test cell

Crossflow bench-scale test cell with recycle loop was previously studied by Kilduff et al. [11]. This system consists of a stainless steel test cell (SEPA, Osmonics) that houses a single membrane sheet of 0.014 m^2 with a maximum operating pressure of 1,000 psi. A high-pressure stainless steel piston feed pump (30 mL min^{-1} at 3000 psi, Eldex, model CC-100-S-4 (no. 19351), Napa, CA, USA) was used for membrane operating pressures while a high capacity booster recycle pump (Gear pump: Model 75211-35, Cole–Parmer Instrument, Vernon Hills, IL, USA) was used to adjust a high crossflow velocity in the recycle loop. Hydraulic hand pump was used to hold the system pressure at the top of bench-scale test cell. Mesh feed spacer was used to create hydrodynamic flow conditions similar to that employed in full-scale spiral-wound elements. For each experiment, inlet temperature was approximately 25 °C under constant atmosphere environment. Recovery was operated at 85% during filtration experiments, and crossflow velocity of 0.1 m s^{-1}, similar to that of full-scale membrane [12], corresponding to a flowrate of 530 mL min^{-1} in the recycle loop.

3.5. Filtration experiments

Membrane sheets were initially rinsed with cleaned DI water and then transferred to the bench-scale test cell. The membrane sheets were then cleaned with citric acid solution of pH 3–4, and followed with sodium hydroxide solution of pH 10 for 30 min each. The system was rinsed with cleaned DI water and was subsequently tested for 30-min membrane compaction with initial water flux of 45 LMH (L m^{-2} h^{-1}). Clean water flux, J_0, was subsequently determined before NOM solution was used to the system.

Prior to filtration experiments, a 200-mL solution having NOM and each scalant was initially used to flush the crossflow bench-scale system without system operating pressure. The piston feed pump was subsequently used to adjust an initial solution flux about 45 LMH and water recovery of 85% ($Q_p/Q_f = 0.85$). The transmembrane pressure was initially recorded and kept constant during filtration experiments. Permeate and retentate flow was periodically measured by using analytical balance (Model BL-2200H, Shimadzu, Japan) in order to determine solution flux and recovery throughout filtration experiments. Permeate and retentate samples were collected to determine total organic carbon (TOC) and conductivity rejection. After filtration termination (500 min), two steps of cleaning were performed; firstly, a hydrodynamic cleaning, and secondly, a chemical cleaning. For hydrodynamic cleaning, DI water was used to recirculate in the recycle loop for 30 min with increasing crossflow velocity of 0.25 m s^{-1}, higher than the velocity of operation. After the cleaning, clean water flux was determined with operating pressures. For chemical cleaning, DI water with pH of 10 (using NaOH) and followed with pH of 3 (using HCl), was used to recirculate the system for 30 min each. Clean DI water was flushed to clean the system and water flux associated with operating pressures was then determined.

4. Results and discussion

4.1. Influence of monovalent and divalent cations on solution flux

Mono- and di-valent cations can cause fouling effects on nanofiltration membrane [2,3]. Fig. 1 presents the influence of monovalent and divalent cations of chloride salts on solution flux. Dot points were the experimental data while solid lines were fitted with fouling models of crossflow operation. It was observed that monovalent (Na^+) and divalent (Ca^{2+}) cations caused flux reduction from 26.1% (I.S. NaCl of 0.01 M) to 35.2% (I.S. $CaCl_2$ of 0.05 M). Solutions containing $CaCl_2$ showed greater flux decline than that containing NaCl. This finding indicated that calcium ion has a marked effect on membrane fouling. Similar results were observed by Hong and Elimelech [3] and Schafer et al. [2]. For monovalent cation, the experimental results were fitted with pore blocking model (at low ionic strength of 0.01 M), possibly due to reduced charge repulsion between positively charged Na^+ and negatively charged membrane, thus affecting membrane surface and/or pores. At high ionic strength of 0.05 M NaCl, the results were followed with cake formation. This was possibly dominated by reduced charge repulsion between positively charged Na^+ and negatively charged NOM, thus resulting an increase of NOM accumulation on the membrane surface. However, an increase of ionic strength from 0.01 to 0.05 M can also decrease charge repulsion between positively charged Na^+ and negatively charged membrane. Table 1 shows rejection data of monovalent and divalent inorganic scalants. From this table, it was observed that the

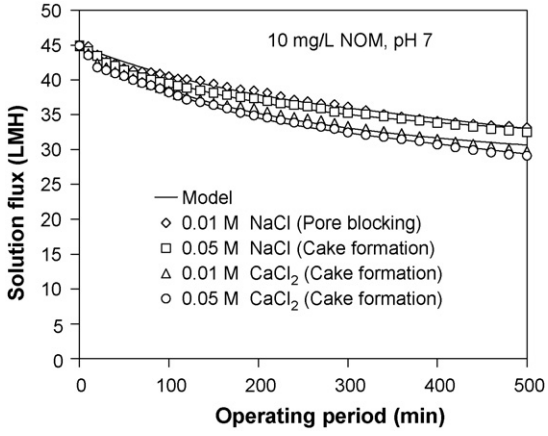

Fig. 1. Influence of monovalent and divalent inorganic scalants on solution flux.

Table 1
Rejection data of monovalent and divalent inorganic scalants

Type of solution	R_r (%)	DOC rejection (%)
0.01 M NaCl	25.3	94.9
0.05 M NaCl	13.7	95.3
0.01 M $CaCl_2$	24.4	97.0
0.05 M $CaCl_2$	38.2	95.7

retentate rejection (R_r) of conductivity decreased from 25.3% to 13.7% with increasing ionic strength from 0.01 to 0.05 M. This can possibly decrease double layer thickness on membrane matrix as reported by Braghetta et al. [13]. The retentate rejection of dissolved organic carbon (DOC) was about 94.9–95.3%. For divalent cation, the effect of calcium ion and NOM interaction could dominate solution flux decline on the membrane surface. This was observed that the retentate rejection of conductivity increased from 24.4% to 38.2%, while the retentate rejection of DOC decreased slightly from 97% to 95.7% with increasing ionic strength from 0.01 to 0.05 M. This was possibly due to calcium and NOM interaction occurred on the membrane surface.

Table 2 shows the model parameters from fouling models for monovalent and divalent cations. It was observed that the experimental data were relatively fitted with cake formation model for calcium chloride solution (both low and high ionic strength). These results were based on minimizing sum squared errors (SSEs) between experimental data and estimated data from fouling models ($\sum(J_{v(model)} - J_{v(measured)})^2$). However, the SSEs were not significantly different for each fouling model.

4.2. Influence of inorganic scalants on solution flux

Fig. 2 illustrates the influence of inorganic scalants on solution flux (I.S. = 0.01 M). Inorganic scalants used in this study were chloride (Cl^-), carbonate (CO_3^{2-}), sulphate (SO_4^{2-}), and phosphate (PO_4^{3-}) with interaction of positively charged

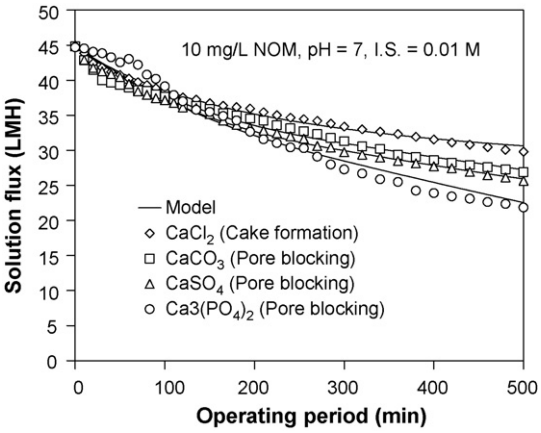

Fig. 2. Influence of inorganic scalants on solution flux (I.S. = 0.01 M).

calcium ion. It was observed that solutions having different inorganic scalants exhibited different solution flux decline. As expected, solution having phosphate species showed the greatest flux decline while solution having chloride species exhibited the least flux decline. The relative flux declines ($1 - J/J_0$) were estimated about 33.6%, 40%, 43%, and 51.1% for Cl^-, CO_3^{2-}, SO_4^{2-}, and PO_4^{3-} species, respectively. Based on mathematical fouling models, the experimental data were relatively fitted with pore blocking model for all solutions having CO_3^{2-}, SO_4^{2-}, and PO_4^{3-} scalants, suggesting inorganic scalants accumulated on the membrane surface and/or pores, thus dominating solution flux curve.

Table 3 shows model parameters from fouling models for inorganic scalants (I.S. = 0.01 M). For each mathematical fouling model, pore blocking model was fitted well with experimental data based on minimized SSEs for CO_3^{2-}, SO_4^{2-}, and PO_4^{3-} species. However, for phosphate species, the minimized SSEs for pore blocking model were relatively different from those of other mathematical models. This suggests that pore

Table 2
Model parameters from fouling models for monovalent and divalent inorganic scalants

Concentration	Pore blocking			Pore constriction			Intermediate			Cake formation		
	k_A (h^{-1})	J^* (LMH)	SSE	k_B ($m^{-0.5}\,h^{-0.5}$)	J^* (LMH)	SSE	k_C (m^{-1})	J^* (LMH)	SSE	k_D ($h\,m^{-2}$)	J^* (LMH)	SSE
0.01 M NaCl	0.246	32.3	5.31	0.968	30.2	5.756	4.5	29.5	5.41	108	29	5.474
0.05 M NaCl	0.355	33.1	3.895	1.5	32	5.683	7.08	31.6	4.906	156	30.6	3.693
0.01 M $CaCl_2$	0.337	30.5	6.406	1.41	28.9	8.925	6.96	28.6	7.765	153	27	5.955
0.05 M $CaCl_2$	0.343	29.6	6.716	1.44	27.9	8.684	6.84	27.2	7.389	150	25.3	5.645

Table 3
Model parameters from fouling models for inorganic scalants (I.S. = 0.01 M)

Concentration	Pore blocking			Pore constriction			Intermediate			Cake formation		
	k_A (h^{-1})	J^* (LMH)	SSE	k_B ($m^{-0.5}\,h^{-0.5}$)	J^* (LMH)	SSE	k_C (m^{-1})	J^* (LMH)	SSE	k_D ($h\,m^{-2}$)	J^* (LMH)	SSE
0.01 M $CaCl_2$	0.337	30.5	6.406	1.41	28.9	8.925	6.96	28.6	7.765	153	27	5.955
0.01 M $CaCO_3$	0.307	27.2	24.81	1.23	24.31	27.55	8.34	26.81	33.96	216	26.36	38.26
0.01 M $CaSO_4$	0.31	25.9	8.386	1.52	24.88	13.136	8.34	25.3	19.781	212	24.97	30.424
0.01 M $Ca_3(PO_4)_2$	0.212	19.9	66.92	1.35	21.21	153.8	6.48	19.9	170.8	165.7	19.81	244.2

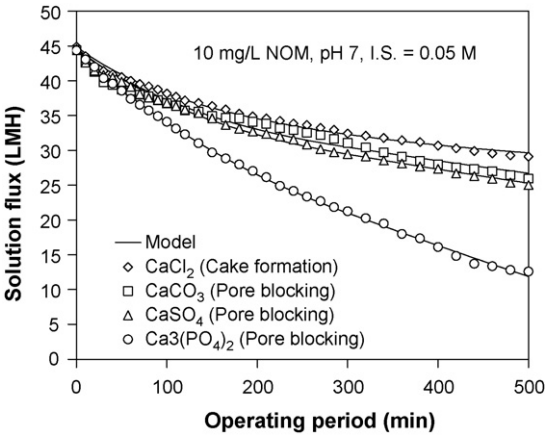

Fig. 3. Influence of inorganic scalants on solution flux (I.S. = 0.05 M).

blocking model is effective in controlling solution flux decline. These experimental results were possibly due to decreased membrane pores from inorganic fouling on membrane surface/pores, thus reduced permeate volume. However, this phenomena was not significantly affected with solution having calcium chloride, possibly due to cake formation from Ca–NOM interaction dominating solution flux curve.

Fig. 3 exhibits the influence of inorganic scalants on solution flux (I.S. = 0.05 M). Experimental results showed similar trend with low ionic strength of 0.01 M. From this figure, it was obvious that solution having phosphate scalant showed the greatest flux decline. The relative flux declines ($1 - J/J_0$) were estimated about 35.2%, 41.6%, 43.9%, and 71.6% for Cl^-, CO_3^{2-}, SO_4^{2-}, and PO_4^{3-} species, respectively. An increase of ionic strength from 0.01 to 0.05 M increased flux decline from 51.1% to 71.6% for phosphate species.

Table 4 shows model parameters from fouling models for inorganic scalants (I.S. = 0.05 M). Based on minimized SSEs, the pore blocking model was relatively fitted well with the experimental data of CO_3^{2-}, SO_4^{2-}, and PO_4^{3-} species. This indicated that inorganic scalants showed significant effect on membrane fouling, thus increased solution flux decline. Solutions having phosphate species had greater solution flux decline than those of other species. The solution flux (J^*) associated with the back-transport mass transfer was approximately 6.34 LMH based on mathematical pore blocking model while the solution fluxes (J^*) were about 26.7 and 25.25 LMH for solutions having carbonate and sulphate species, respectively. This exhibited significant differences between inorganic species on nanofiltration fouling.

For ionic strength of 0.01 and 0.05 M, solution flux curves seemed to follow the same order of the solubility product constants (K_{sp}) (Cl^-, SO_4^{2-} ($10^{-4.7}$), CO_3^{2-} ($10^{-8.34}$), and PO_4^{3-} (i.e. $10^{-54.1}$) species) within the first 100-min operation. However, solution flux declines of SO_4^{2-} species seemed to cross these of CO_3^{2-} species after the 100-min operation. Based on solubility product constants, solution having 0.01 M CO_3^{2-} species could initially form $CaCO_{3(s)}$ in the feed stream, thus affecting solution flux decline. Solution having 0.01 M SO_4^{2-} species (0.00233 M $CaSO_4$ and 0.0007 M NaCl) contained lower

Table 4
Model parameters from fouling models for inorganic scalants (I.S. = 0.05 M)

Concentration	Pore blocking			Pore constriction			Intermediate			Cake formation		
	k_A (h^{-1})	J^* (LMH)	SSE	k_B ($m^{-0.5}\,h^{-0.5}$)	J^* (LMH)	SSE	k_C (m^{-1})	J^* (LMH)	SSE	k_D ($h\,m^{-2}$)	J^* (LMH)	SSE
0.05 M $CaCl_2$	0.343	29.6	6.716	1.44	27.9	8.684	6.84	27.2	7.389	150	25.3	5.645
0.05 M $CaCO_3$	0.309	26.7	27.09	1.27	24.13	31.13	8.22	26	35.52	223.9	25.9	41
0.05 M $CaSO_4$	0.305	25.25	6.979	1.32	22.8	9.285	8.46	25.1	22.59	223.8	24.91	37.55
0.05 M $Ca_3(PO_4)_2$	0.19	6.34	2.847	1.13	6.74	59.94	6.76	8.07	145	179.6	3.81	279.5

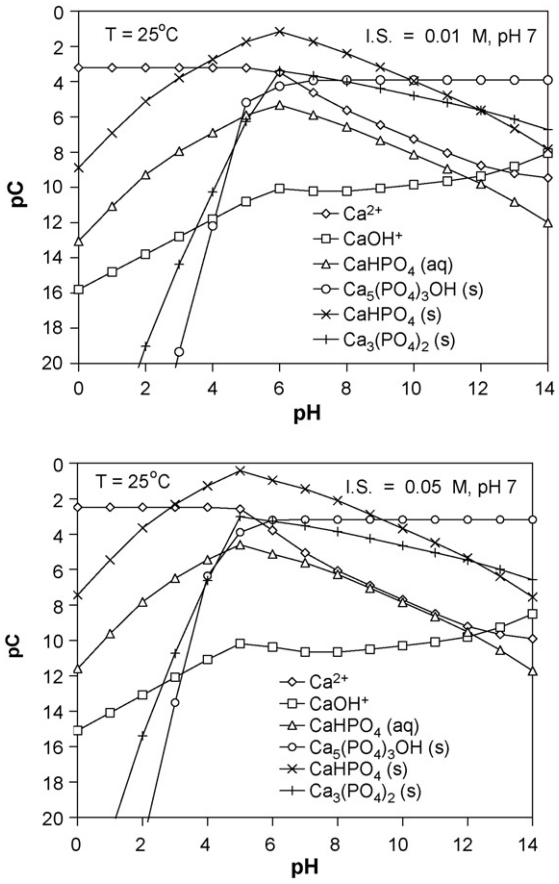

Fig. 4. The pC–pH diagram on calcium phosphate scalant.

concentration than solubility equilibrium (0.00447 M). This may result no precipitated sulfate species formed on the membrane surface at the beginning of the experiment. After the period of 100-min operation, the concentration of solution having sulfate species exceeded the solubility limit causing the scaling $CaSO_{4(s)}$ deposited on the membrane surface due to rejected species, thus increased concentration polarization on the membrane surface. This could possibly dominate solution flux curve by inducing sulfate scaling deposited on the membrane, thus lower flux curve than that of CO_3^{2-} species. At the period of 120-min operation, it was observed that the conductivity for SO_4^{2-} species in the retentate stream was about 2.67 times higher than that in the feed stream. This may enhance concentration polarization on the membrane surface. In addition, the conductivity rejection for SO_4^{2-} species was about 72.7% higher than that for CO_3^{2-} species about 48.6%. This could possibly affect the solution flux curve after 100-min operation, especially at high ionic strength of 0.05 M, where both precipitated species already formed. Solution having PO_4^{3-} species showed greater flux reduction with increasing ionic strength from 0.01 to 0.05 M, possibly due to precipitated species easily formed on the membrane surface. This could be related to the lowest solubility product constant for PO_4^{3-} species.

Fig. 4 exhibited the pC–pH diagram on calcium phosphate scalant. The concentration lines were analyzed based on MINEQL+ program for chemical equilibrium system. For both low and high ionic strength, phosphate scalant showed higher concentrations of precipitated species than those of dissolved species. The precipitated species could be $CaHPO_{4(s)}$, $Ca_5(PO_4)_3OH_{(s)}$, and $Ca_3(PO_4)_{2(s)}$, which showed relatively high concentration. However, the concentrations of these species were dependent on pH value. From this figure, the precipitated species could be $Ca_5(PO_4)_3OH_{(s)}$ if the pH of solution was greater than 10. The solubility product constants were reported as follows [14]:

$$CaHPO_{4(s)} \Leftrightarrow Ca^{2+} + HPO_4^{2-}, \quad K_{sp} = 3 \times 10^{-7}$$

$$Ca_5(PO_4)_3OH_{(s)} \Leftrightarrow 5Ca^{2+} + 3PO_4^{3-} + OH^-,$$
$$K_{sp} = 8 \times 10^{-55}$$

$$Ca_3(PO_4)_{2(s)} \Leftrightarrow 3Ca^{2+} + 2PO_4^{3-}, \quad K_{sp} = 1 \times 10^{-27}$$

It was observed that the solubility products of phosphate species were relatively low, thus indicating the capacity of phosphate precipitation on membrane surface. It was noticed that solution flux curve was relatively fitted with pore blocking model for most divalent inorganic scalants. This suggested that divalent inorganic scalants could form precipitated species due to relatively high ion concentrations, thus suggesting a precipitated fouling on membrane surface and/or pores, thus decreasing permeate volume.

4.3. Influence of different divalent inorganic scalants on solution flux

Fig. 5 shows the influence of different divalent inorganic scalants on solution flux. Calcium and magnesium represents different divalent species, which interact with sulphate inorganic scalants for both low and high ionic strengths. It was observed that solution flux curve of calcium species showed greater flux decline than that of magnesium species for both low and high ionic strengths. An increase of ionic strength from 0.01 to 0.05 M showed no significant effect on solution flux for both calcium sulphate and magnesium sulphate. The relative flux declines $(1 - J/J_0)$ of calcium were determined about 43% and

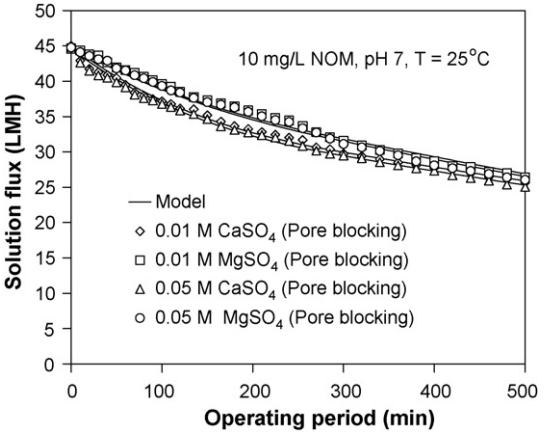

Fig. 5. Influence of divalent inorganic scalants on solution flux.

Table 5
Model parameters from fouling models for different divalent inorganic scalants

Concentration	Pore blocking			Pore constriction			Intermediate			Cake formation		
	k_A (h^{-1})	J^* (LMH)	SSE	k_B ($m^{-0.5}\,h^{-0.5}$)	J^* (LMH)	SSE	k_C (m^{-1})	J^* (LMH)	SSE	k_D ($h\,m^{-2}$)	J^* (LMH)	SSE
0.01 M $CaSO_4$	0.31	25.9	8.386	1.52	24.88	13.136	8.34	25.3	19.781	212	24.97	30.424
0.01 M $MgSO_4$	0.194	24.04	13.07	0.93	22.98	27.66	4.68	22.21	36.63	103.8	19.91	51.67
0.05 M $CaSO_4$	0.305	25.25	6.979	1.32	22.8	9.285	8.46	25.1	22.59	223.8	24.91	37.55
0.05 M $MgSO_4$	0.203	23.98	12.54	0.934	22.31	24.91	4.8	21.83	35.62	108	19.34	50.87

43.9% for ionic strengths of 0.01 and 0.05 M, respectively. For magnesium, the relative flux declines ($1 - J/J_0$) were estimated about 40.9% and 41.8% for ionic strengths of 0.01 and 0.05 M, respectively. Based on mathematical fouling model, pore blocking model was relatively fitted with experimental data for both inorganic species.

Table 5 presents model parameters from fouling models for different divalent inorganic scalants. It was observed that pore blocking model showed minimized SSEs compared with other mathematical fouling models (i.e. pore constriction, intermediate, and cake formation). The results indicate that precipitated species dominated solution flux decline when compared with Ca–NOM interaction forming cake on membrane surface.

Fig. 6 presents the pC–pH diagram on calcium sulphate scalant. For low ionic strength of 0.01 M, precipitated species ($CaSO_4{\cdot}2H_2O_{(s)}$ and $CaSO_{4(s)}$) showed relatively high concentrations on membrane surface. It was possible that the precipitated species ($CaSO_4{\cdot}2H_2O_{(s)}$ and $CaSO_{4(s)}$) could cause membrane fouling corresponding to the mathematical fouling model based on pore blocking model. This suggests a reduction of membrane pores, thus decreased permeate volume. For high ionic strength of 0.05 M, the precipitated species ($CaSO_{4(s)}$) could easily form due to higher concentration than the $CaSO_4{\cdot}2H_2O_{(s)}$ species.

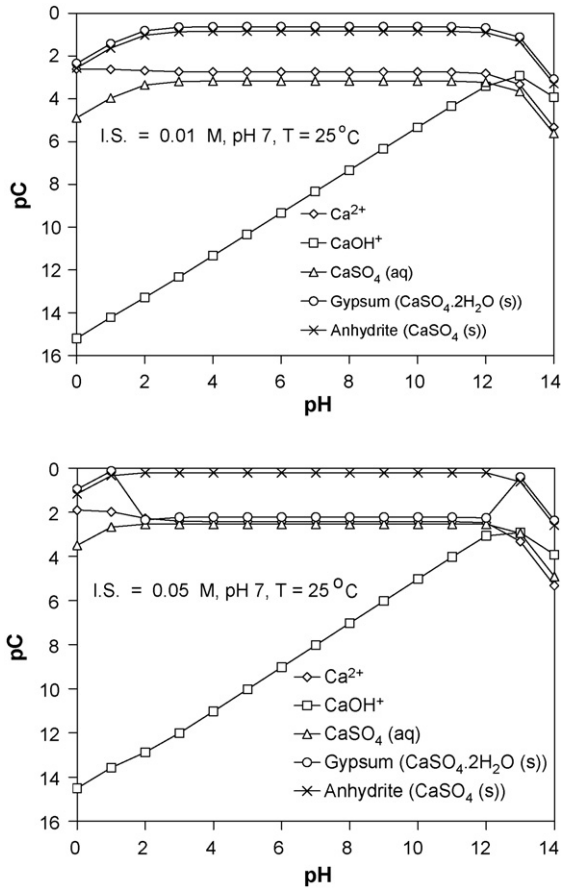

Fig. 6. The pC–pH diagram on calcium sulphate scalant.

The different forms of precipitated species were possibly dependent on solubility-product constants. It was reported that the solubility-product constants of $CaSO_{4(s)}$, $CaSO_4{\cdot}2H_2O_{(s)}$, and $CaSO_{4(aq)}$ [15] were as follows [14,15]:

$$CaSO_{4(s)}\,(\text{anhydrite}) \Leftrightarrow Ca^{2+} + SO_4{}^{2-}, \quad K_{sp} = 10^{-4.7}$$

$$CaSO_4{\cdot}2H_2O_{(s)}\,(\text{gypsum}) \Leftrightarrow Ca^{2+} + SO_4{}^{2-} + 2H_2O, \quad K_{sp} = 10^{-4.58}$$

$$CaSO_{4(aq)} \Leftrightarrow Ca^{2+} + SO_4{}^{2-}, \quad K_{sp} = 10^{-2.23}$$

It was observed that the solubility-product constants of $CaSO_{4(s)}$ and $CaSO_4{\cdot}2H_2O_{(s)}$ were relatively low about $10^{-4.7}$ and $10^{-4.58}$, respectively. The dissolved $CaSO_{4(aq)}$ species had relatively high solubility-product constant (about $10^{-2.23}$). This suggests that the precipitated species could be easily formed when compared with the dissolved $CaSO_{4(aq)}$ species. For low ionic strength of 0.01 M, the precipitated $CaSO_4{\cdot}2H_2O_{(s)}$ species could be easily formed based on high concentration in the pC–pH diagram while the precipitated $CaSO_{4(s)}$ could dominate on membrane surface for high ionic strength of 0.05 M.

Fig. 7 presents the pC–pH diagram on magnesium sulphate scalant. For low ionic strength of 0.01 M and pH 7, dissolved magnesium species (Mg^{2+}) had higher concentration than precipitated species (i.e. epsomite ($MgSO_4{\cdot}7H_2O_{(s)}$) and $Mg(OH)_{2(s)}$). However, the precipitated magnesium species of $Mg(OH)_{2(s)}$ had higher concentration than that of Epsomite ($MgSO_4{\cdot}7H_2O_{(s)}$), when pH was greater than 9. For high ionic strength of 0.05 M, the concentrations of dissolved magnesium (Mg^{2+}), ($Mg(OH)_{2(s)}$), and epsomite ($MgSO_4{\cdot}7H_2O_{(s)}$) were not significantly different when pH was about 7. However, at high ionic strength of 0.05 M, the precipitated species of $MgSO_4{\cdot}7H_2O_{(s)}$ showed greater concentration than that of low ionic strength of 0.01 M, but solution flux curves of low and high ionic strength exhibited no significant difference. The experimental results suggested that precipitated species of $MgSO_4{\cdot}7H_2O_{(s)}$ could be formed on the membrane surface because the experimental data were relatively fitted well with pore blocking model. However, the precipitated magnesium

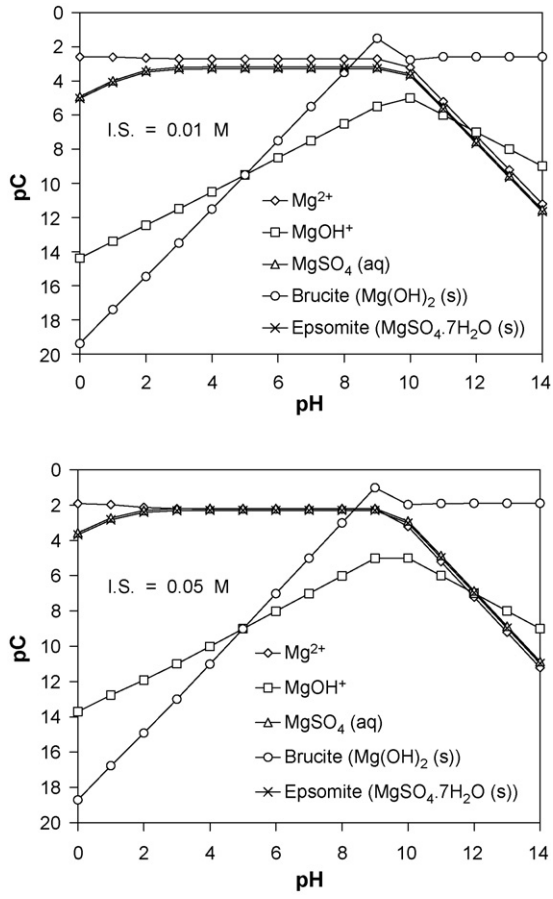

Fig. 7. The pC–pH diagram on magnesium sulphate scalant.

species showed no significant effect on solution flux and presented less solution flux decline than the precipitated calcium.

5. Conclusions

The influence of inorganic scalants and NOM on NF fouling was dependent on number of ion valency (monovalent and divalent cations), types of inorganic scalants (chloride, carbonate, sulphate, and phosphate) and different divalent inorganic scalants (calcium and magnesium). Mathematical fouling models were successfully used to determine kinetics and fouling mechanisms on the NF membrane surface while the pC–pH diagram could be used to interpret experimental results. For chloride inorganic scalant, solution flux curve of divalent cation (Ca^{2+}) showed greater flux decline than that of monovalent cation (Na^{+}). For divalent cation, experimental data were relatively fitted well with cake formation model, while experimental results dominated cake formation model for monovalent cation (Na^{+}) with high ionic strength of 0.05 M. This was possibly caused by charge interaction between positive charges (Na^{+} and/or Ca^{2+}) and negatively charged NOM, thus increasing NOM mass accumulation on the membrane surface. For carbonate, sulphate, and phosphate scalants, pore blocking model dominated solution flux curve, suggesting precipitated species accumulated on membrane surface and/or pores, thus decreased solution flux. Phosphate scalant showed greater flux decline than sulfate and carbonate scalants for both low and high ionic strength, suggesting easily formed a precipitated phosphate scalant on the membrane surface and/or pores. The precipitated phosphate species would be $CaHPO_{4(s)}$, $Ca_5(PO_4)_3OH_{(s)}$, and $Ca_3(PO_4)_{2(s)}$, which showed relatively high concentration based on the pC–pH diagram of calcium phosphate scalant for both low and high ionic strengths. For different divalent inorganic scalants (calcium and magnesium), calcium showed greater flux decline than magnesium, possibly due to higher concentration of precipitated calcium species than that of precipitated magnesium species based on the pC–pH diagram. The results exhibited the possibility of pore blocking model dominating solution flux decline for most polyprotic anions. However, for calcium chloride, the interaction between NOM and calcium can play an important role in solution flux decline, thus causing cake formation mechanism on the membrane surface.

Acknowledgements

The authors would like to thank the Thailand Research Fund (TRF) and the Commission on Higher Education, Thailand, for financial support.

References

[1] A. Seidel, M. Elimelech, Coupling between chemical and physical interaction in natural organic matters (NOM) fouling of nanofiltration membranes: implications for fouling control, J. Membr. Sci. 203 (2002) 245–255.
[2] A.I. Schafer, A.G. Fane, T.D. Waite, Nanofiltration of natural organic matter: removal, fouling and the influence of multivalent ions, Desalination 118 (1998) 109–122.
[3] S. Hong, M. Elimelech, Chemical and physical aspects of natural organic matter (NOM) fouling of nanofiltration membranes, J. Membr. Sci. 132 (1997) 159–181.
[4] P. Dydo, M. Turek, J. Ciba, Scaling analysis of nanofiltration systems fed with saturated calcium sulfate solutions in the presence of carbonate ions, Desalination 159 (2003) 245–251.
[5] J. Hermia, Constant pressure blocking filtration laws: application to power-law non-Newtonian fluids, Trans. Inst. Chem. Eng. 60 (1982) 183–187.
[6] W.R. Bowen, J.I. Calvo, A. Hernandez, Steps of membrane blocking in flux decline during protein microfiltration, J. Membr. Sci. 101 (1995) 153–165.
[7] R.W. Field, D. Wu, J.A. Howell, B.B. Gupta, Critical flux concept for microfiltration fouling, J. Membr. Sci. 100 (1995) 259–272.
[8] W. Peng, I.C. Escobar, D.B. White, Effects of water chemistries and properties of membrane on the performance and fouling—a model development study, J. Membr. Sci. 238 (2004) 33–46.
[9] L. Sun, E.M. Perdue, J.F. McCarthy, Using reverse osmosis to obtain organic matter from surface and ground waters, Water Res. 29 (6) (1995) 1471–1477.
[10] S.M. Serkiz, E.M. Perdue, Isolation of dissolved organic matter from the Suwannee river using reverse osmosis, Water Res. 24 (7) (1990) 911–916.
[11] J.E. Kilduff, S. Mattaraj, G. Belfort, Flux decline during nanofiltration of naturally occurring dissolved organic matter: effects of osmotic pressure, membrane permeability, and cake formation, J. Membr. Sci. 239 (1) (2004) 39–53.
[12] S.C. Allgeier, R.S. Summers, Evaluating NF for DBP control with the RBSMT, J. AWWA 87 (3) (1995) 87–99.
[13] A. Braghetta, F.A. DiGiano, W.P. Ball, Nanofiltration of natural organic matter: pH and ionic strength effects, J. Environ. Eng.: ASCE 123 (7) (1997) 628–641.
[14] C.N. Sawyer, P.L. McCarty, G.F. Parki, Chemistry for Environmental Engineering and Science, 5th ed., McGraw-Hill, NY, USA, 2003.
[15] J.I. Drever, The Geochemistry of Natural Waters, 2nd ed., Prentice Hall, NJ, USA, 1988.